Armstrong and Chan[28] is strikingly similar to that of the $S_1$ state of PS II, measured by Klein and co-workers.[47] Since the $S_2$-state EPR spectrum can be simulated with either a $(III)_3(IV)$ or $(III)(IV)_3$ tetramer,[37,48] the assignment supported by the BVS results is also consistent with the EPR results. It should be noted, however, that while the tetranuclear formulation is gaining increasing support and appears extremely likely to be correct,[41] there are other models which, though rather cumbersome, have not been definitively ruled out. If the tetranuclear formulation does not survive continued experimentation, the BVS results may have to be reconsidered. Nevertheless, the method should still be applicable in light of any new information that may become available in the future.

## Conclusions

The bond valence sum method is a powerful tool in analyzing the compatibility of a given set of crystallographically determined bond distances with a particular metal oxidation state.[9] The calculations performed for the model complexes show that the method can be applied to crystallographically determined distances in metalloenzymes that have also been determined using EXAFS. This presents the intriguing possibility that the method may be used to gain insight into metalloprotein active sites that have been studied by EXAFS. The values in Table III suggest that the method works quite well for a variety of structures, including mixed-valence units and complex ligation environments such as those found in the oxo-bridged diiron enzymes.

When applied to the Mn cluster in PS II, the BVS method can distinguish between assignment of the tetramer to the $(III)_4$, $(II)_2(IV)_2$, or $(IV)_4$ oxidation states in $S_1$. The calculated BVS's are most compatible with the $(III)_2(IV)_2$ assignment and can account for the failure of the average Mn–O bond distance to decrease significantly upon oxidation of one of the Mn centers to form the $S_2$ state. Since EXAFS is such a powerful technique for determining bond lengths, the BVS method presents a potentially attractive complement to XANES analysis for determining oxidation states of metal centers in metalloproteins.

**Acknowledgment.** I thank Drs. G. W. Brudvig, C. C. Torardi, and J. E. Penner-Hahn for helpful discussions; the donors of the Petroleum Research Fund, administered by the American Chemical Society, for financial support; the Camille and Henry Dreyfus Foundation for a New Faculty Award; the National Science Foundation for a Presidential Young Investigator Award; and the David and Lucile Packard Foundation for a Fellowship in Science and Engineering.

(47) Dexheimer, S. L.; Sauer, K.; Klein, M. P. In *Current Research in Photosynthesis*; Baltscheffsky, M., Ed.; Kluwer: Dordrecth, The Netherlands, 1990; p 761.
(48) Brudvig, G. W. In *Advanced EPR*; Hoff, A. J., Ed.; Elsevier: New York, 1989; p 839.

---

Contribution from the Inorganic Chemistry Laboratory, University of Oxford, South Parks Road, Oxford OX1 3QR, U.K., Chemistry Department, University of Manchester, Manchester M13 9PL, U.K., and SERC Daresbury Laboratory, Daresbury, Warrington WA4 4AD, U.K.

# Variable Photon Energy Photoelectron Spectroscopy of $OsO_4$ and Pseudopotential Calculations of the Valence Ionization Energies of $OsO_4$ and $RuO_4$

Jennifer C. Green,*,† Martin F. Guest,§ Ian H. Hillier,‡ Stephen A. Jarrett-Sprague,‡ Nikolas Kaltsoyannis,† Michael A. MacDonald,§ and Kong H. Sze†

*Received August 6, 1991*

Relative partial photoionization cross sections and photoelectron branching ratios have been obtained for the valence bands of osmium tetraoxide in the ionization energy range 12–18 eV. The photon energies used ranged between 24 and 115 eV. The ionization cross sections of the $2t_2$, 1e, and $2a_1$ orbitals show evidence of substantial metal character. By use of an ab initio many-body Green's function formalism that takes into account the effect of electron correlation and relaxation, ionization energies of $OsO_4$ and $RuO_4$ have been calculated. Considerations of the spectral features and the predictions of the calculation lead to an assignment of ion state ordering of $^2T_1 < {}^2T_2 < {}^2A_1 < {}^2E < {}^2T_2$. The presence of a substantial p–d resonance feature in the cross section of the upper $^2T_2$ and $^2E$ ion states shows that the $2t_2$ and 1e orbitals have significant Os 5d character. The lower $^2T_2$ ion state (arising from ionization from the $3t_2$ orbital) undergoes a spin–orbit splitting of 0.4 eV resulting from an Os 6p contribution to the $3t_2$ molecular orbital.

## Introduction

The volatility, high symmetry, and classic character of $OsO_4$ led to both this molecule and the closely related $RuO_4$ being early targets in the application of gas-phase photoelectron spectroscopy (PES) to the study of bonding in transition metal complexes.[1-5] $RuO_4$ proved a difficult candidate for investigation as both $CO_2$ and $H_2O$ accompanied the spectrum in the early stages of measurement and the electron multipliers were attacked, leading to poor instrumental performance.[1-4] Once the ambiguities, due to impurities, in the number of spectral bands were resolved there was general agreement on the correlation of bands between the two compounds. Various assignments were proposed for the spectra of these two compounds, which are summarized along with the ionization energies (IEs) in Table I. Subsequently, two theoretical papers concurred[6,7] in revising the assignment of the photoelectron (PE) spectrum of $OsO_4$. These assignments are also given in Table I. Details of the various empirical arguments

**Table I.** Ionization Energies and Assignments of the PE Spectra of $OsO_4$ and $RuO_4$

| | vertical IE/eV[a] | | ref | | | | |
|---|---|---|---|---|---|---|---|
| band | $OsO_4$ | $RuO_4$ | 1[b] | 2 | 3, 4 | 6 | 7 |
| 1 | 12.35 | 12.15 | $^2T_1$ | $^2T_2$ | $^2T_1$ | $^2T_1$ | $^2T_1$ |
| 2 | 13.14 | 12.92 | $^2T_2(U')$ | $^2T_1$ | $^2T_2$ | $^2T_2$ | $^2T_2$ |
| 3 | 13.54 | 13.01 | $^2T_2(E'')$ | $^2A_1$ | $^2E$ | $^2A_1$ | $^2A_1$ |
| 4 | 14.66 | 13.93 | $^2E$ | $^2E$ | $^2A_1$ | $^2E$ | $^2E$ |
| 5 | 16.4, 16.8 | 16.1 | $^2T_2$ | $^2T_2$ | $^2T_2$ | $^2T_2$ | $^2T_2$ |

[a] IE values are taken from refs 3 and 4, where IE values for the observed vibrational fine structure are also given. [b] Diemann and Muller assigned the $^2A_1$ ion state to a band at 15.58 eV in the spectrum of $OsO_4$ and one at 15.50 eV in the spectrum of $RuO_4$. These bands were subsequently shown to be from an impurity.

† University of Oxford.
‡ University of Manchester.
§ SERC Daresbury Laboratory.

(1) Diemann, E.; Müller, A. *Chem. Phys. Lett.* **1973**, *19*, 538.

0020-1669/92/1331-1588$03.00/0 

for band assignment will be discussed below.

Measurement of PE cross sections of ionization bands over a wide range of photon energies provides empirical evidence for the localization of the ionizing electrons.[8-11] Not only can d-bands be readily identified by this means[8-11] but also evidence for d- and f-orbital covalency can be obtained.[9-11] It therefore seemed appropriate to study the PE spectrum of $OsO_4$ over a wide range of photon energies using synchrotron radiation in order to clarify the spectral assignment and to obtain further information on the bonding in this prototypical molecule. A preliminary report on this PE study has already appeared.[12] As $RuO_4$ had had a deleterious effect on electron detectors, it was not considered a suitable candidate for study, as the channel plates in our spectrometer appear to be particularly sensitive to chemical attack.

The discrepancy between the generally accepted experimental assignment of the valence ionizations and the theoretical predictions suggested that a theoretical reinvestigation might also be enlightening. We report pseudopotential calculations on $OsO_4$ and $RuO_4$ and their ionization energies obtained by use of an ab initio many-body Green's function formalism.

## Experimental Section

A sample of $OsO_4$ was obtained commercially from Johnson and Matthey. Its He I spectrum was compared with that reported previously,[4] and the sample was judged to be sufficiently pure to use without further purification.

The photoelectron spectra of $OsO_4$ were obtained using the synchrotron source at the SERC Daresbury Laboratory. A full account of our experimental method has been given,[8] and the apparatus and its performance is described elsewhere;[13] therefore, only a brief account of experimental procedures is given here.

Synchrotron radiation from the 2-GeV electron storage ring at the SERC Daresbury Laboratory was monochromated using a toroidal grating monochromator (TGM) and was used to photoionize gaseous samples in a cylindrical ionization chamber. The TGM was employed with fixed slit widths of 2 mm. Total instrumental resolution was limited by the electron pass energy and was in the range 150–600 meV. The photoelectrons were energy analyzed with a three-element zoom lens in conjunction with a hemispherical electron energy analyzer, which was positioned at the "magic angle" in order to eliminate the influence of the photoelectron asymmetry parameter, $\beta$, on signal intensity. Multiple-scan PE spectra were collected at each photon energy required. The decay of the storage ring beam current was corrected for by linking the scan rate with the output from a photodiode positioned to intersect the photon beam after it had passed through the gas cell. The sensitivity of the photodiode to different radiation energies was determined by measuring the $np^{-1}$ PE spectra of Ne, Ar, and Xe. These were also used to characterize and correct for a fall off in analyzer collection efficiency at kinetic energies <15 eV. Photoionization cross sections for the rare gases were taken from the literature.[14,15]

$OsO_4$ was sufficiently volatile that it could be attached outside the spectrometer and sublimed at ambient temperatures into the gas cell via the same line as the inert gases. A liquid-nitrogen-cooled finger was fitted to the spectrometer to prevent diffusion of compound into the pumps.

Sample pressure fluctuations were corrected for by collecting a "standard" calibration spectrum before and after each data spectrum.

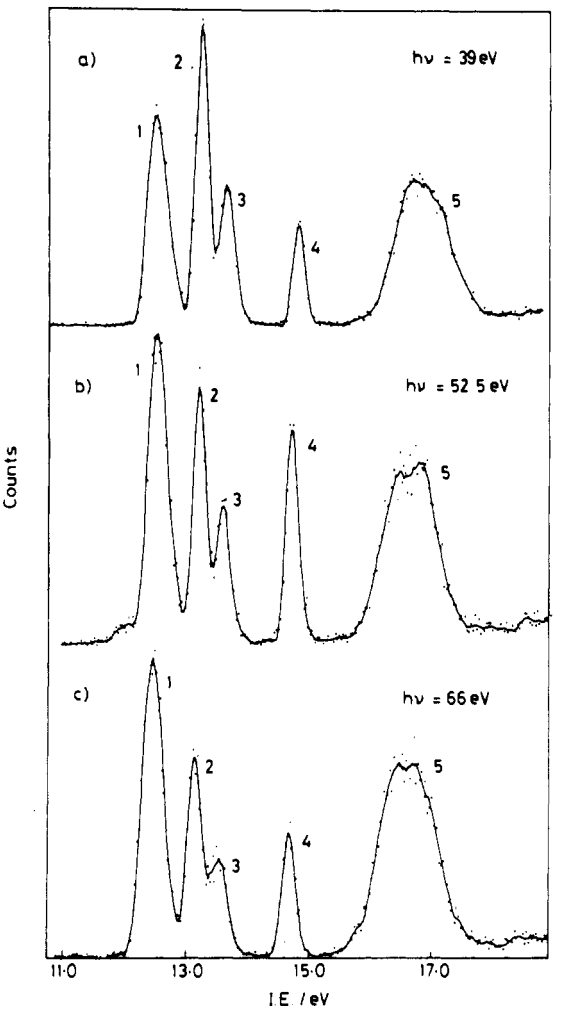


**Figure 1.** Photoelectron spectra of $OsO_4$ at (a) 39, (b) 52.5, and (c) 66 eV of photon energy.

The integrated intensities of the bands in these spectra were then used as a relative measure of the sample density in the ionization region.

## Computation

The calculations employed effective core potentials for both osmium and oxygen. The oxygen pseudopotential was the compact effective potential of Stevens et al.,[16] and the relativistic pseudopotential for osmium was from Hay and Wadt.[17] For comparison we have performed calculations on $RuO_4$. The valence basis was of triple-$\zeta$ quality. For oxygen, the basis was that of Stevens et al.,[16] while for osmium the double-$\zeta$ basis of Hay and Wadt was expanded by replacing each of the most diffuse s, p, and d functions by two such functions. These s, p, and d exponents were (0.117, 0.029), (0.058, 0.015), and (0.293, 0.0732) respectively. For ruthenium, the double-$\zeta$ basis of Hay and Wadt was similarly expanded with s, p, and d functions having exponents of (0.083, 0.021), (0.050, 0.013) and (0.300, 0.075), respectively. All calculations were performed using the program GAMESS[18] on the FPS M64/60 of the Computational Chemistry Group of Manchester University.

Calculations were performed with experimental metal–oxygen bond lengths of $OsO_4$ (1.711 Å)[19] and $RuO_4$ (1.706 Å).[19] At the lowest level the IEs were obtained by using Koopmans' approximation. Electron relaxation and correlation were then included in more accurate estimates of the IEs by use of a Green's function proceedure. Here the two-particle-hole Tamm–Dancoff (2ph-TDA) method[20] was employed using 12 filled and 32 virtual orbitals. We have previously found that this method is particularly useful in calculating IEs of transition metal complexes,

(2) Foster, S.; Phelps, S.; Cusachs, L. C.; McGlynn, S. P. *J. Am. Chem. Soc.* **1973**, *95*, 5521.
(3) Evans, S.; Hamnett, A.; Orchard, A. F. *J. Chem. Soc.* **1974**, *96*, 6221.
(4) Burroughs, P.; Evans, S.; Hamnett, A.; Orchard, A. F.; Richardson, N. V. *J. Chem. Soc. Faraday Trans. 2* **1974**, *70*, 1895.
(5) Egdell, R. G. *D. Phil. Thesis*, University of Oxford 1977.
(6) Rauk, A.; Ziegler, T.; Ellis, D. E. *Theor. Chim. Acta* **1974**, *34*, 49.
(7) Weber, J. *Chem. Phys. Lett.* **1977**, *45*, 261.
(8) Cooper, G.; Green, J. C.; Payne, M. P.; Dobson, B. R.; Hillier, I. H. *J. Am. Chem. Soc.* **1987**, *109*, 3836.
(9) Cooper, G.; Green, J. C.; Payne, M. P. *Mol. Phys.* **1988**, *63*, 1031.
(10) Brennan, J. G.; Green, J. C.; Redfern, C. M. *J. Am. Chem. Soc.* **1989**, *111*, 2373.
(11) Brennan, J. G.; Green, J. C.; Redfern, C. M.; MacDonald, M. A. *J. Chem. Soc., Dalton Trans.* **1990**, 1907.
(12) Green, J. C.; Kaltsoyannis, N.; Sze, K. H.; MacDonald, M. A. *Chem. Phys. Lett.* **1990**, *175*, 359.
(13) Potts, A. W.; Novak, I.; Quinn, F.; Marr, G. V.; Dobson, B. R.; Hillier, I. H. *J. Phys. B* **1985**, *18*, 3177.
(14) West, J. B.; Marr, G. V. *Proc. R. Soc. London, A* **1976**, *349*, 347.
(15) West, J. B.; Morton, J. *At. Data Nucl. Data Tables* **1978**, *22*, 103.
(16) Stevens, W. J.; Basch, H.; Krauss, M. *J. Chem. Phys.* **1984**, *81*, 6026.
(17) Hay, P. J.; Wadt, W. R. *J. Chem. Phys.* **1985**, *82*, 270.
(18) Guest, M. F. *GAMESS User's Guide*; SERC (Daresbury Laboratory): Daresbury, U.K., 1990.
(19) Krebs, B.; Hasse, K. D. *Acta Crystallogr.* **1976**, *B32*, 1334.
(20) von Niessen, W.; Schirmer, J.; Cederbaum, L. S. *Comput. Phys. Rep.* **1989**, *1*, 57.

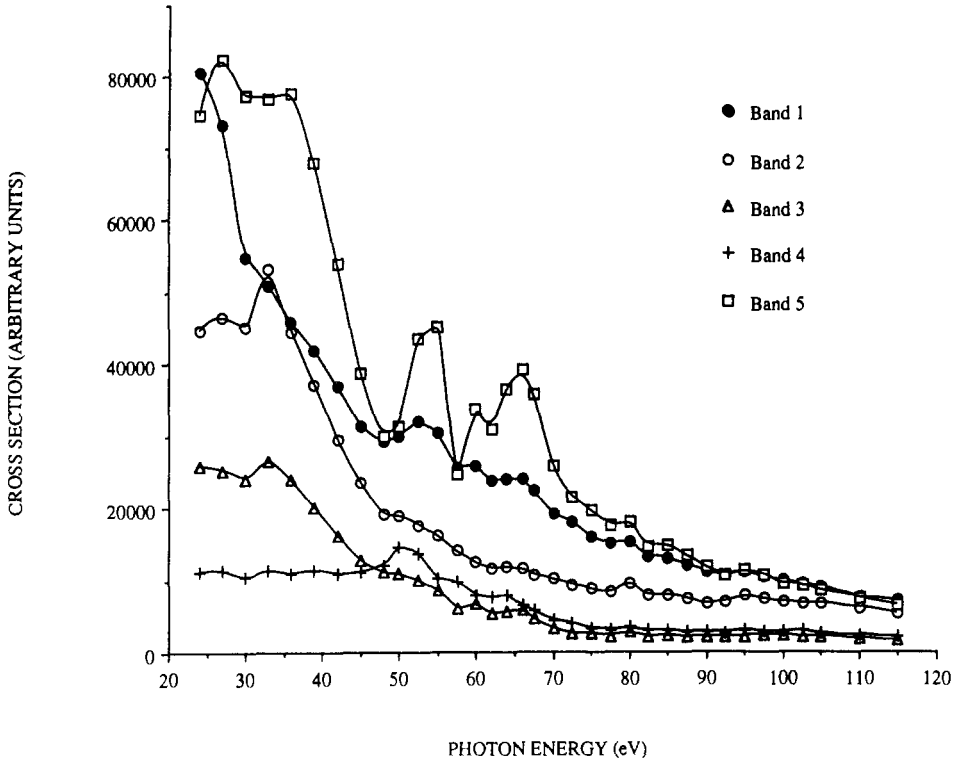


**Figure 2.** Relative partial photoionization cross sections of bands 1–5 in the photoelectron spectrum of $OsO_4$.

where differential relaxation effects are important.[21] We also calculated the IEs by performing ΔSCF–CI calculations on the ground state and the ion states of $OsO_4$, with which we compare and contrast the results from the 2ph-TDA method. The ΔSCF–CI calculations were performed using single and double excitations from 12 filled and 29 virtual orbitals.

Spin–orbit coupling constants were calculated by Dr. N. Edelstein using the procedures of Cowan.[22]

## Results

The PE spectra of $OsO_4$, obtained at photon energies of 39, 52.5, and 66 eV are shown in Figure 1. We did not attempt to resolve the vibrational fine structure seen in previous He I studies.[2,3] Consequently, the bands had an asymmetric shape and it proved necessary to use asymmetric Gaussian functions to fit the peaks, and thus obtain the band areas used in the relative partial photoionization cross section (RPPICS) calculations. The RPPICS for bands 1–5 in the PE spectrum of $OsO_4$ are given in Figure 2, and expanded plots of each band are presented in Figure 3.

The most pronounced feature is the "double hump" profile of the cross section data for band 5 in the region 50–70 eV. This is a clear indication of p–d giant resonant enhancement[23] of the cross section of this band, coinciding with the Os 5p subshell ionization potentials ($^2P_{3/2}$ = 49 eV, $^2P_{1/2}$ = 61 eV).[24] This behavior is expected from molecular orbitals (MOs) having significant Os 5d character. Between 24 and 37 eV of photon energy, the cross section of band 5 passes through a maximum. This is a common feature of d ionizations, the delayed maximum being due to centrifugal barriers preventing the continuum f-wave from occupying the inner well region.[24] Calculations on atomic ionization cross sections for Os 5d orbitals[25] predict the maximum to occur at a kinetic energy (KE) of 15.1 eV, which is similar to the KE of ~14 eV we find for the cross section maximum of band 5. Both these features suggest that band 5 arises from ionization from an orbital (or orbitals) with significant d character.

The RPPICs of band 4 maintains a fairly constant level between photon energies of 24–44 eV. Between 44 and 55 eV there is a strong intensity rise and fall with a maximum at ca. 50 eV. Though this coincides with the region of the 5p $^2P_{3/2}$ ionization, the absence of a second stronger resonance between 55 and 70 eV leads us to discount a p → d resonance followed by super Coster–Kronig decay as its origin. At higher photon energies the cross section falls off sharply. Overall the very different cross section behavior of band 4 in comparison with bands 1–3 leads us to support the assignment of this band to the $2a_1^{-1}$ ionization. Sharp $a_1^{-1}$ ionization bands which show relative intensity increases in He II as opposed to He I spectra are found in the PE spectra of transition metal tetrahalides.[26] The cross section features of band 4 may well reflect a significant Os 6s contribution to the MO; a Cooper minimum is predicted for the Os 6s cross section around 40 eV[25] so that a maximum at 50 eV may well reflect the recovery of the cross section after such a minimum. Alternatively the maximum may be due to a molecular shape resonance.[27] Photoionization from an $a_1$ orbital involves a $t_2$ ionization channel. As such a channel is also accessible to electrons ionizing from the other MOs, an explanation on shape resonance grounds implies that for other ionizations the effect is relatively less important.

The cross section behavior of band 1 is rather different from that of bands 2 and 3 whose RPPICS resemble one another. The renormalized branching ratios (BRs) of bands 2 and 3 are presented in Figure 4, and are very close to 2:1 in the spectra acquired with photon energies below 70 eV. Above this photon energy the ratio increases to a value of ~3.5:1, but this change may well be an artifact of the fitting; above 70 eV, a higher pass energy is used for the electron analysis, and the resolution deteriorates. All three bands show small intensity fluctuations between 55 and 70 eV in the same region as band 5, though the features are much weaker. Within the three bands the maxima are most pronounced for band 1. Such p → d resonances have been observed previously for ionization bands from orbitals which, by symmetry, may have no metal d character,[9] but they are normally

(21) Burton, N. A.; Hillier, I. H.; Kendrick, J. *Chem. Phys. Lett.* **1989**, *155*, 195.
(22) Cowan, R. D. *The Theory of Atomic Structure and Spectra*: Chemical Abstracts Service: Columbus, OH, 1981.
(23) Dehmer, J. L.; Starace, A. F.; Fano, U.; Sugar, J.; Cooper, J. W. *Phys. Rev. Lett.* **1971**, *26*, 1521.
(24) Briggs, D., Ed. *Handbook of X-ray and Ultraviolet Photoelectron Spectroscopy*; Heyden; London, 1977.
(25) Yeh, J. J.; Lindau, I. *At. Data Nucl. Data Tables* **1985**, *32*, 1.
(26) Egdell, R. G.; Orchard, A. F. *J. Chem. Soc., Faraday Trans. 2* **1978**, *74*, 485.
(27) Robin, M. B. *Chem. Phys. Lett.* **1985**, *119*, 33.

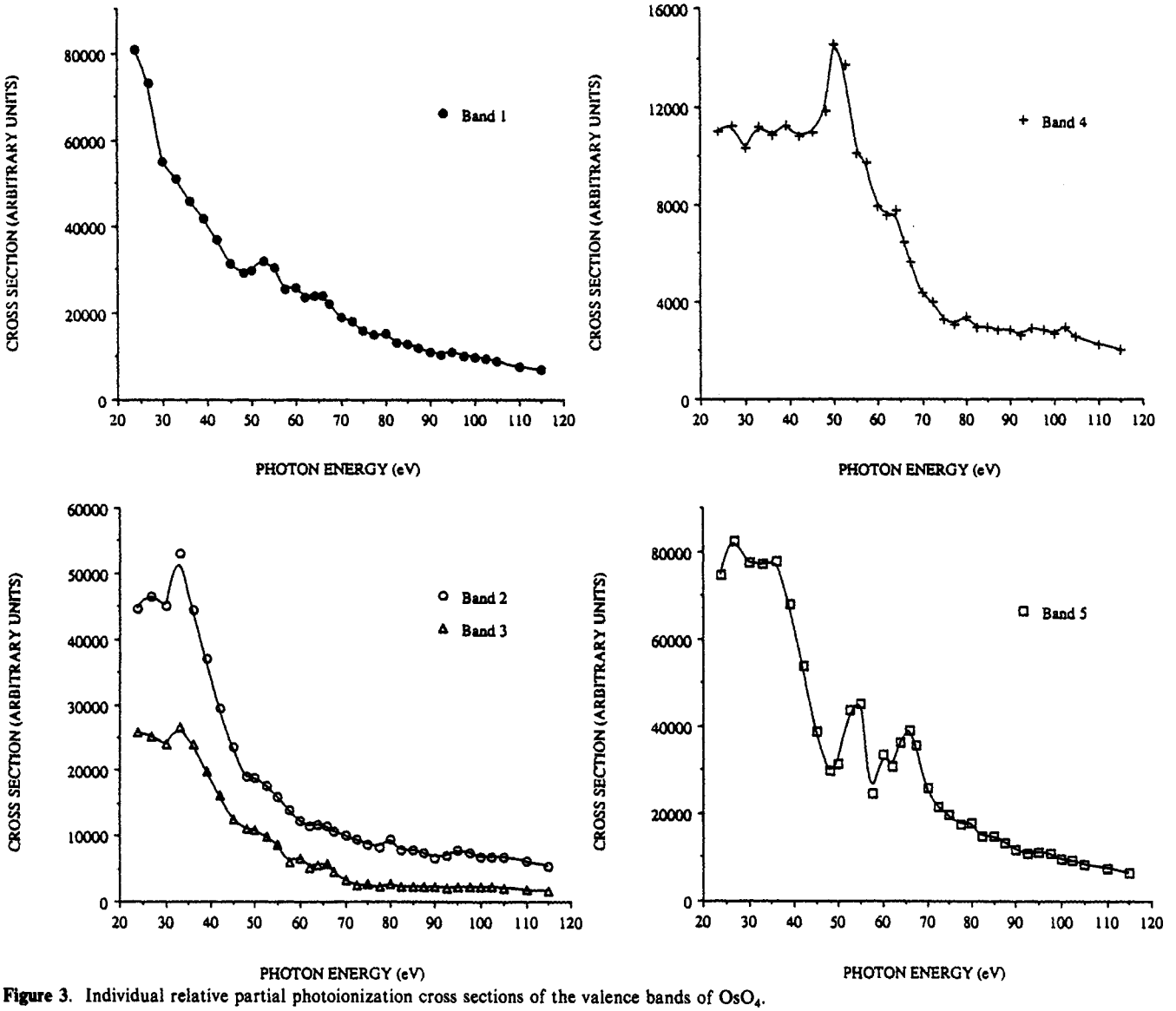


**Figure 3.** Individual relative partial photoionization cross sections of the valence bands of $OsO_4$.

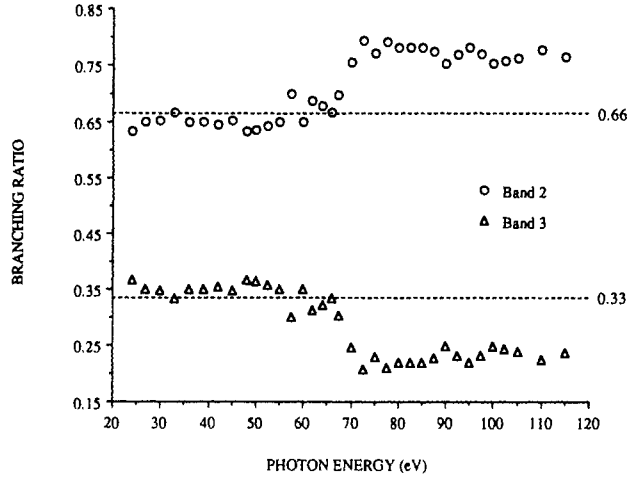


**Figure 4.** Renormalized photoelectron branching ratios for bands 2 and 3 of $OsO_4$. Dotted lines illustrate the 2:1 ratio of bands 2 and 3 in the region where the spectra are well resolved.

weaker than from those associated with orbitals in which d character is symmetry allowed.

The calculations of the IEs are summarized in Table II. There is good agreement between the IEs of $OsO_4$ calculated by the 2ph-TDA method and those obtained using the ΔSCF–CI approach. The IEs for $OsO_4$ and $RuO_4$ are in broad agreement with a somewhat smaller separation between the 1e and $2t_2$ ionizations for the latter molecule.

**Table II.** Calculated Ionization Energies (eV) for $OsO_4$ and $RuO_4$

| | MO | calcd IE: Koopmans | calcd IE: 2ph-TDA | calcd IE: ΔSCF–CI | band assignt[a] |
|---|---|---|---|---|---|
| $OsO_4$ | $1t_1$ | 14.2 | 12.4 | 11.7 | 1 |
| | $3t_2$ | 15.8 | 13.6 | 13.2 | 2, 3 |
| | $2a_1$ | 16.3 | 14.7 | 14.4 | 4 |
| | $2t_2$ | 20.6 | 17.6 | *b* | 5 |
| | 1e | 21.0 | 18.0 | 18.2 | 5 |
| $RuO_4$ | $1t_1$ | 14.6 | 12.7 | | |
| | $3t_2$ | 15.5 | 13.5 | | |
| | $2a_1$ | 15.3 | 13.9 | | |
| | $2t_2$ | 20.8 | 18.9 | | |
| | 1e | 21.0 | 18.9 | | |

[a] See Figure 1. [b] The SCF method can only obtain the lowest state of a particular symmetry.

## Discussion

The valence electronic structures of the $d^0$ tetrahedral $MO_4$ species are of the form

$$(1a_1)^2(1t_2)^6(2t_2)^6(2a_1)^2(1e)^4(3t_2)^6(1t_1)^6$$

(where the numbering scheme ignores orbitals correlating with the core orbitals of the constituent atoms). A schematic MO diagram showing the possible atomic contributions to the various MOs is given in Figure 5. $1a_1$ and $1t_2$ are essentially O 2s orbitals.

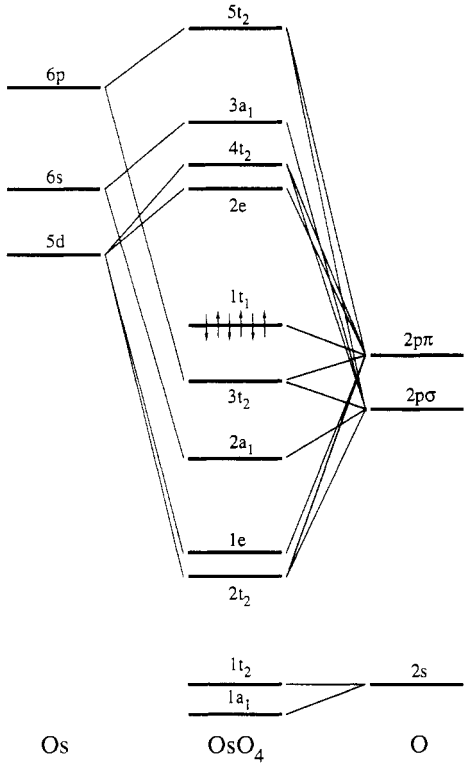


**Figure 5.** Schematic molecular orbital diagram for $OsO_4$.

Of the other occupied levels $2t_2$ and $2a_1$ are traditionally associated with M–O $\sigma$-bonding and 1e and $3t_2$ with M–O $\pi$-bonding, though there is strictly no $\sigma/\pi$ separability among the $t_2$ set of MOs. The $1t_1$ orbital, in the absence of any effective f-orbital contribution from the central atom, is nonbonding. For a $d^0$ tetrahedral molecule, such as $OsO_4$, five primary ion states are expected to occur in the ionization region studied, namely a $^2A_1$, a $^2E$, and a $^2T_1$ state and two $^2T_2$ states. However, more than five bands may well be observed as the orbitally degenerate states may be subject to Jahn–Teller distortion or spin–orbit splitting.

Previous results on the vibrational structure of the bands are summarized here.[1-5] Bands 1–4 all show resolved vibrational structure. This is most complex in 1 where the band system is dominated by a progression of mean interval ca. 900 (±80) $cm^{-1}$, which is assigned to the $a_1$ stretch and which has a frequency of 965 $cm^{-1}$ in the ground state of $OsO_4$.[28] Furthermore, there is a second progression of interval ca. 300 (±80) $cm^{-1}$ representing excitation of either a $t_2^4$ or e mode[1] (323 and 333 $cm^{-1}$ respectively for $OsO_4$[28]). Bands 2–4 exhibit fine structure due to an $a_1$ mode with intervals of 900–950 $cm^{-1}$, just less than that of neutral $OsO_4$. The similarity of the vibrational fine structure of bands 2 and 3 is particularly striking.

Band 5 is broad with no resolvable fine structure but has two distinct maxima about 0.4 eV apart. The relative areas of the two parts of the band are approximately 1:2. As this splitting is too great for a simple vibrational progression, three alternative interpretations are possible. Either band 5 correlates with two primary ion states, or it is a $^2T$ state split by either Jahn–Teller or spin–orbit coupling.

The previous report on the synchrotron study[12] took as the assignment of band 5 a spin–orbit split $^2T_2$ ion state. This leads to the conclusion that there is very little $\pi$-bonding in $OsO_4$ as bands 2 and 3, which are then assigned to $^2T_2$ and $^2E$ ion states, respectively, and arise from the $\pi$ type orbitals, show negligible d character. This is sufficiently contrary to most other evidence that further theoretical investigation was required as described in this paper.

The results of the calculations reported here strongly suggest that band 5 must be assigned to both $^2T_2$ and $^2E$ ion states, which restores the picture of significant $\pi$ bonding as the e orbital is shown to be both tightly bound and to have a high d content (Table III). If 5 does arise from two separate states then two of the bands 1–4 must also arise from the same state with the degeneracy lifted by one of the possible mechanisms. Only band 1 shows a Jahn–Teller active vibrational mode, bands 2–4 showing a progression due to an $a_1$ stretch. Furthermore, Jahn–Teller splittings of degenerate ion states of the magnitude found for the separations of bands 1–4 are accompanied by much more extensive vibronic structure than is found here. Methane, for example, where the $t_2$ orbitals are strongly bonding, has a $^2T_2$ ionization band with maxima separated by ca. 0.8 eV and extensive structure,[29] whereas the U′ component of the nonbonding $t_1$ ionization of $CBr_4$ shows a splitting of 0.09 eV and no extensive vibronic structure.[30] Not one of the MOs giving rise to bands 1–4 is strongly bonding. We therefore conclude that the spectral appearance is inconsistent with the production of four well-separated bands from three primary ion states by a Jahn–Teller mechanism.

**Table III.** Orbital Characteristics (Mulliken Population Analysis) of $OsO_4$ and $RuO_4$

| | | metal | | | oxygen | |
|---|---|---|---|---|---|---|
| | MO | s | p | d | s | p |
| $OsO_4$ | $1t_1$ | 0.000 | 0.000 | 0.000 | 0.000 | 0.250 |
| | $3t_2$ | 0.000 | 0.046 | 0.014 | 0.003 | 0.232 |
| | $2a_1$ | 0.172 | 0.000 | 0.000 | 0.013 | 0.194 |
| | $2t_2$ | 0.000 | 0.023 | 0.432 | 0.023 | 0.113 |
| | 1e | 0.000 | 0.000 | 0.492 | 0.000 | 0.127 |
| $RuO_4$ | $1t_1$ | 0.000 | 0.000 | 0.000 | 0.000 | 0.250 |
| | $3t_2$ | 0.000 | 0.031 | 0.019 | 0.002 | 0.235 |
| | $2a_1$ | 0.034 | 0.000 | 0.000 | 0.010 | 0.232 |
| | $2t_2$ | 0.000 | 0.000 | 0.479 | 0.021 | 0.103 |
| | 1e | 0.000 | 0.025 | 0.524 | 0.000 | 0.118 |

**Table IV.** Energy Ordering of Spin–Orbit Multiplets for $^2T_2$ States

| | | configuration | |
|---|---|---|---|
| | | $t_2^1$ | $t_2^5$ |
| orbital origin of splitting | p | E″ < U′ | U′ < E″ |
| | d | U′ < E″ | E″ < U′ |

The most likely candidate for a spin–orbit split pair of bands are bands 2 and 3. They have identical vibrational fine structure and show a constant 2:1 branching ratio over the photon energy range where the bands are well resolved (20–70 eV). The separation of bands 2 and 3 is 0.4 eV in $OsO_4$ and 0.09 eV in $RuO_4$, consistent with an increase in spin–orbit splitting with atomic number of the central atom. No other pair of bands fulfils these necessary conditions. Orchard et al.[3,4] rule out the possibility of 2 and 3 being spin–orbit components arising from an Os 5d contribution to the $3t_2$ MO, as a $t_2$ hole state gives rise to the sequence of multiplet states E″ < U′[30,31] (as is found for example in the d band ionization of $W(CO)_6$[32]). But band 2 is twice as intense as band 3, giving a multiplet ordering which is qualitatively incorrect. Also the RPPICS data determined here shows minimal 5d character in the orbitals giving rise to bands 2 and 3, and the calculation predicts approximately 1% d character (Table III).

The ordering of spin–orbit multiplets for $^2T_2$ states is given in Table IV. Spin–orbit splitting could also originate from an Os 6p contribution to the $3t_2$ MO. For a hole in a p shell ($p^5$ configuration), the spin–orbit multiplet ordering is U′ < E″ (as is found for the 6p ionizations of Xe with $^2P_{3/2} < {}^2P_{1/2}$).

The multiplet splitting should be

$$^3/_2c^2\zeta_{6p}$$

(28) McDowell, R.; Goldblatt, M. *Inorg. Chem.* **1971**, *10*, 625.

(29) Turner, D. W.; Baker, C.; Baker, A. D.; Brundle, C. R. *Molecular Photoelectron Spectroscopy*; Wiley-Interscience: London, 1970.

(30) Green, J. C.; Green, M. L. H.; Joachim, P. J.; Orchard, A. F.; Turner, D. W. *Philos. Trans. R. Soc. London A* **1970**, *268*, 111.

(31) Griffiths, J. S. *The Theory of Transition Metal Ions*; Cambridge University Press: Cambridge, U.K., 1961.

(32) Higginson, B. R.; Lloyd, D. R.; Burroughs, P.; Gibson, D. M.; Orchard, A. F. *J. Chem. Soc., Faraday Trans. 2* **1973**, *74*, 234.

**Table V.** Calculation of Spin–Orbit Constants for Osmium 6p[33]

| ion | configuration | $\zeta_{6p}$/eV Blume–Watson[a] | $\zeta_{6p}$/eV R*VI[b] |
|---|---|---|---|
| Os | $[Xe]4f^{14}5d^{6}6s^{1}6p^{1}$ | 0.294 | 0.298 |
| $Os^{+}$ | $[Xe]4f^{14}5d^{6}6p^{1}$ | 0.456 | 0.462 |
| $Os^{2+}$ | $[Xe]4f^{14}5d^{5}6p^{1}$ | 0.715 | 0.725 |
| $Os^{3+}$ | $[Xe]4f^{14}5d^{4}6p^{1}$ | 0.979 | 0.992 |
| $Os^{4+}$ | $[Xe]4f^{14}5d^{3}6p^{1}$ | 1.237 | 1.255 |
| $Os^{5+}$ | $[Xe]4f^{14}5d^{2}6p^{1}$ | 1.500 | 1.521 |
| $Os^{6+}$ | $[Xe]4f^{14}5d^{1}6p^{1}$ | 1.765 | 1.789 |
| $Os^{7+}$ | $[Xe]4f^{14}6p^{1}$ | 2.032 | 2.060 |

[a] $\zeta_{6p}$ calculated by the Blume–Watson method; see p 94 in ref 22. [b] $\zeta_{6p}$ calculated with eq 8.2 in ref 22.

where $c$ is the coefficient of the Os 6p orbital in the $3t_2$ MO and $\zeta_{6p}$ is the 6p spin–orbit coupling constant. The calculation (Table III) predicts a 5% 6p contribution to the $3t_2$ MO of $OsO_4$. Estimates[33] of $\zeta_{6p}$ for Os in various configurations have been obtained using Cowan's proceedure.[22] The results are given in Table V. Mulliken population analysis suggests a configuration between $d^4$ and $d^5$ for Os in $OsO_4$ (Table III). The rough prediction of the U′–E″ splitting is therefore 0.064 eV. This is considerably less than the observed value of 0.4 eV but the theoretical estimates are somewhat crude, a higher charge on the Os together with a higher 6p contribution to the $3t_2$ MO could increase the estimate significantly, but it would need say 18% 6p character and a $d^2$ configuration to produce the observed splitting of 0.4 eV.

The $3t_2$ $\sigma$-bonding level of $Pb(CH_3)_4$ shows a multiplet splitting of 0.91 eV; given a value of $\zeta_{6p}$ for Pb of 1.16 eV a 52% contribution from the Pb 6p orbital to the $3t_2$ MO can be estimated.[34] In this case the band is broad, suggesting unresolved vibrational structure consistent with significant bonding character implied by such a high Pb contribution. An alternative conceivable source of spin–orbit coupling is the Os core 5p orbitals mixing with the $3t_2$ level. Such an effect has been observed for actinide tetrahalides.[35] However, actinide 6p levels lie much closer to the valence shell ionizing at typically 25 and 33 eV for Th and 24 and 34 eV for U,[24] whereas Os 5p levels ionize at 49 and 61 eV.[24] It seems likely that they are too deeply buried in the core for such a perturbation to be significant.

One consequence of assigning bands 2 and 3 to a $^2T_2$ state is that band 1 must arise from the $^2T_1$ ion state. The very small p–d resonance in this band[12] results from inter-channel coupling[36] as there can be no d-orbital contribution to the $t_1$ MO.

From the calculation (see Table II), the MOs with the most similar character are the $1t_1$ and $3t_2$ orbitals which are principally O 2p. For this pair of ionizations, therefore, we might expect the cross sections to be most similar. In the photon energy region 70–115 eV, where resonance effects are expected to be minimal and the cross sections should be dominated by the AOs, the combined intensity of bands 2 and 3 lies close to that of band 1, in agreement with this expectation.

Though the situation regarding the magnitude of the spin–orbit splitting is not entirely satisfactory, we prefer the assignment

| band | 1 | 2 | 3 | 4 | 5 |
|---|---|---|---|---|---|
| state | $^2T_1$ | U′ ($^2T_2$) | E″ ($^2T_2$) | $^2A_1$ | $^2E$, $^2T_2$ |

The arguments in favor of this choice are the weight of the ion state calculations, the consistency between the experimental evidence of the Os d contribution to the orbitals associated with band 5 and that predicted by the theory for the $2t_2$ and e MOs, and the large body of evidence for multiple bonding, and hence $\pi$-bonding, in $OsO_4$.

**Table VI.** Optimized Os–O Distances (Å) in $OsO_4$ and Its Various Ion States

| | state | bond length |
|---|---|---|
| $OsO_4$ | $^1A_1$ | 1.785 |
| $OsO_4^+$ | $^2T_1$ | 1.777 |
| | $^2T_2$ | 1.743 |
| | $^2A_1$ | 1.813 |
| | $^2E$ | 1.836 |

A further point for comment is the vibrational structure associated with bands 2–4. They all show evidence for excitation of an $a_1$ stretch with the 0–0 transition being the most intense. This is normally cited as evidence of very little geometry change between the molecule and ion and hence of ionization from a nonbonding orbital. However, evidence from the cross section variations, the spin–orbit coupling, and the theoretical calculations suggests that the associated $2a_1$ and $3t_2$ orbitals are bonding and have contributions from the Os 6s and 6p orbitals, respectively. These orbitals are very radially extended so that bond length differences make very little difference to the net ligand overlap in these cases. In contrast, the Os 5d O 2p overlap will be very dependent on metal–ligand distance, and ionization from orbitals from high d character will result in greater vibrational excitation. We have optimized the geometry in the molecule and the various ion states at the SCF level and the resulting Os–O bond lengths are given in Table VI. For the neutral molecule the calculated Os–O bond length (1.79 Å) is in good agreement with the experimental value (1.719 Å). The predicited bond length changes on valence ionization show the expected trend. The largest change is associated with the 1e ionization in line with the large metal character of this MO (Table III), while ionization from the $1t_1$ nonbonding MO results in the smallest bond length change. Both $2a_1$ and $3t_2$ ionization results in significant, though smaller bond length changes, in line with the small metal character of these MOs and in agreement with indications from vibrational structure in the PE spectrum that little geometry change occurs on ionization from the $2a_1$ and $3t_2$ MOs associated with bands 2–4.

Band 1 as well as showing a symmetric vibration progression also exhibits excitation of a Jahn–Teller active mode,[1,2,4] indicating that the associated $^2T_1$ ground state is not tetrahedral. Given the nonbonding nature of the $t_1$ orbital, a possible driving force of the Jahn–Teller distortion is localization of the hole on ionization on one of the oxygen atoms.

Our proposed assignment of the PE spectrum of $OsO_4$ carries over to $RuO_4$ (Table II). Here the U′ and E″ components of the $^2T_2$ state are much closer in energy, being separated by 0.08 eV due to the reduced spin–orbit splitting of Ru 5p. Indeed, for both $OsO_4$ and $RuO_4$, there is excellent agreement between the calculated and measured IEs (Tables I and II) except for the $2t_2$ and 1e ionizations for which the calculated values are too large by circa 2 eV.

The main determinant of the orbital energy ordering is seen to be the nature of the metal orbital contributing to the MO; the e and $t_2$ levels with 5d contribution are the most stable, followed by the $a_1$ orbital with Os 6s character, then the $t_2$ orbital with 6p character, and finally the $t_1$ level with no metal contribution. This contrasts strongly with a model of $\sigma$-orbitals being more stable than $\pi$-orbitals (the pure $\pi$-bonding level, e, being more stable than the $\sigma$-bonding $a_1$ level); there is strong $\sigma$-$\pi$ mixing in the $t_2$ levels.

## Conclusions

The ion state ordering in $OsO_4$ has been shown to be

$$^2T_1 < U'(^2T_2) < E''(^2T_2) < {}^2A_1 < {}^2E < {}^2T_2$$

which is consistent with the results of recently reported symmetry-adapted cluster theories.[37] The 1e and $2t_2$ orbitals have been shown to have substantial Os 5d character, the $2a_1$ orbital Os 6s character and the $3t_2$ orbital Os 6p character. In the latter case the 6p character probably gives rise to spin-orbit splitting of the

(33) Edelstein, N. Personal communication.
(34) Evans, S.; Green, J. C.; Joachim, P. J.; Orchard, A. F.; Turner, D. W.; Maier, J. P. *J. Chem. Soc., Faraday Trans. 2* **1972**, *68*, 905.
(35) Boerrigter, P. M.; Snijders, J. G.; Dyke, J. M. *J. Electron Spectrosc. Relat. Phenom.* **1988**, *46*, 43.
(36) Southworth S. H.; Parr, A. C.; Hardis, J. E.; Dehmer, J. L. *Phys. Rev. A* **1986**, *33*, 1020.
(37) Nakatsuzi, H.; Saito, S. *Int. J. Quantum Chem.* **1991**, *39*, 93.

associated $^2T_2$ ion state. The large Os 5d contribution to and high binding energy of the 1e molecular orbitals supports the traditional view of strong $\pi$-bonding.

**Acknowledgment.** We wish to thank Dr. N. Edelstein for the Os spin–orbit coupling calculations, Dr. P. A. Cox and Professor C. K. Jørgensen for helpful discussions, Prof. W. von Niessen for use of this Green's function program, the Johnson Mathey Chemical Co. for a loan of $OsO_4$, and the SERC for financial support.

Contribution from the Department of Chemistry,
Washington State University, Pullman, Washington 99164-4630

# Spectroscopic, Electrochemical, and Spectroelectrochemical Investigations of Mixed-Metal Osmium(II)/Ruthenium(II) Bimetallic Complexes Incorporating Polypyridyl Bridging Ligands

Mark M. Richter and Karen J. Brewer*

*Received July 30, 1991*

The synthesis, electrochemical, spectroscopic, and spectroelectrochemical properties of $[(bpy)_2Os(BL)Ru(bpy)_2](PF_6)_4$ (where BL = 2,3-bis(2′-pyridyl)pyrazine (dpp), 2,3-bis(2′-pyridyl)quinoxaline (dpq), and 2,3-bis(2′-pyridyl)benzoquinoxaline (dpb) and bpy = 2,2′-bipyridine) are reported. Addition of the $Ru(bpy)_2^{2+}$ moiety to the vacant coordination site on the bridging ligand in the $[Os(bpy)_2BL]^{2+}$ parent compounds results in a shift to lower energies of the metal-to-ligand charge transfer (MLCT) transitions terminating in the bridging-ligand-based $\pi^*$ orbital as well as a shift to more positive potential of the bridging-ligand-based electrochemical reductions. The lowest energy electronic transitions in these mixed-metal systems have been assigned to overlapping $Os(d\pi) \rightarrow BL(\pi^*)$ and $Ru(d\pi) \rightarrow BL(\pi^*)$ $^1$MLCT transitions with the $Os(d\pi) \rightarrow BL(\pi^*)$ transition occurring at slightly lower energies. On the basis of spectroelectrochemical experiments, the first and second reductions of the bimetallic complexes have been assigned to sequential reductions of the bridging ligand.

## Introduction

There has been an increased amount of interest recently in multimetallic polypyridyl complexes which incorporate both osmium and ruthenium.[1,2] Whereas the majority of studies have centered on ruthenium polypyridyl complexes, osmium polypyridyl complexes have also been shown to have interesting spectroscopic and electrochemical properties.[3] Also, osmium appears to have several advantages over ruthenium. For example, the excited state chemistry of ruthenium is strongly affected by low-lying dd states which tend to complicate the interpretation of the photophysical and photochemical properties and have been known to lead to photodecomposition.[4] The dd states in osmium are much higher in energy than in ruthenium and many of the problems associated with ruthenium can be bypassed or avoided.

Within this framework we have synthesized compounds of general form $[(bpy)_2Os(BL)Ru(bpy)_2]^{4+}$, where BL = dpp, dpq, and dpb. These ligands are similar to bpy but have the added ability to coordinate additional metal centers through the remote nitrogens, making possible the development of multimetal systems.

**Table I.** Cyclic Voltammetric Data for Bimetallic Polypyridyl-Bridged Os(II)/Ru(II) Complexes

| complex | solvent | $E_{1/2}$,[a] V | | |
|---|---|---|---|---|
| $[(bpy)_2Os(dpp)Ru(bpy)_2]^{4+}$ | $CH_3CN$ | +1.56 | +1.01 | |
| | DMF | −0.62 | −1.03 | −1.34 |
| | | −1.41 | −1.61 | −1.74 |
| $[(bpy)_2Os(dpq)Ru(bpy)_2]^{4+}$ | $CH_3CN$ | +1.61 | +1.09 | |
| | DMF | −0.33 | −0.94 | −1.32 |
| | | −1.42 | −1.56 | −1.73 |
| $[(bpy)_2Os(dpb)Ru(bpy)_2]^{4+}$ | $CH_3CN$ | +1.62 | +1.09 | |
| | DMF | −0.21 | −0.76 | −1.34 |
| | | −1.42 | −1.59 | −1.75 |

[a] Potentials were recorded versus a Ag/AgCl reference electrode (0.268 V vs SHE) in 0.1 M $Bu_4NPF_6$ at a scan rate of 200 mV/s.

These three ligands differ from each other only by the addition of electron-withdrawing benzene groups fused to the side of the pyrazine ring. This results in a net stabilization of the lowest-unoccupied $\pi^*$ orbital. Also, this series of ligands, like the non-bridging bpy ligand, provide diimine coordination to the metal center. This makes possible the development of a series of compounds in which properties that are not directly related to the BL-based orbital energies are not significantly altered by bridging-ligand substitution.

The mono- and bimetallic complexes reported herein clearly demonstrate how both the ground-state electrochemical and metal-to-ligand charge-transfer (MLCT) excited-state properties of these mixed-metal systems are dependent upon the nature of the bridging polypyridyl ligand.

## Experimental Section

**Materials.** The materials were reagent grade and used without further purification. The ligands dpq and dpb were synthesized according to literature methods.[5,6] The acetonitrile used in the electrochemical measurements was spectroquality (Burdick and Jackson) and the supporting electrolyte used, tetrabutylammonium hexafluorophosphate

(1) (a) Bock, C. R.; Meyer, T. J.; Whitten, D. G. *J. Am. Chem. Soc.* **1974**, *96*, 4710. (b) Bock, C. R.; Connor, J. A.; Guttierrez, A. R.; Meyer, T. J.; Whitten, D. G.; Sullivan, B. P.; Nagle, J. K. *J. Am. Chem. Soc.* **1979**, *101*, 4815.
(2) Navon, G.; Sutin, N. *Inorg. Chem.* **1974**, *13*, 2159.
(3) See, for example: Sutin, N.; Creutz, C. *Adv. Chem. Ser.* **1978**, *168*, 1. Meyer, T. J. *Acc. Chem. Res.* **1978**, *11*, 94. Sabbatini, N.; Balzani, V. *J. Am. Chem. Soc.* **1972**, *94*, 7587. Demas, J. N.; Adamson, A. W. *J. Am. Chem. Soc.* **1971**, *93*, 1800. Kane-Maguire, N. A. P.; Lagford, C. H. *J. Am. Chem. Soc.* **1971**, *93*, 1800. Balzani, B.; Moggi, L.; Manfrin, M. F.; Bolletta, F.; Lawrence, G. A. *Coord. Chem. Rev.* **1975**, *15*, 321. Lin, C. T.; Sutin, N. *J. Phys. Chem.* **1976**, *80*, 97. Brugger, P. A.; Infelta, P. O.; Brown, A. M.; Gratzel, M. *J. Am. Chem. Soc.* **1981**, *103*, 320. Brewer, K. J.; Murphy, R. W., Jr.; Spurlin, S. R.; Petersen, J. D. *Inorg. Chem.* **1986**, *25*, 882. Hage, R.; Haasnoot, J. G.; Niewenhuis, H. A.; Reedijk, J.; de Ridder, D. J. A.; Vos, J. G. *J. Am. Chem. Soc.* **1990**, *112*, 9245. Barigelletti, F.; De Cola, L.; Balzani, V.; Hage, R.; Haasnoot, J. G.; Reedijk, J.; Vos, J. G. *Inorg. Chem.* **1991**, *30*, 641 and references therein.
(4) (a) Lumpkin, R. S.; Kober, E. M.; Worl, L. A.; Murtaza, Z.; Meyer, T. J. *J. Phys. Chem.* **1990**, *94*, 239. (b) Kober, E. M.; Marshall, J. L.; Dressick, W. J.; Sullivan, B. P.; Caspar, J. V.; Meyer, T. J. *Inorg. Chem.* **1985**, *24*, 2755 and references therein. (c) Pinnick, D.; Durham, B. *Inorg. Chem.* **1984**, *23*, 1440.
(5) Goodwin, H. A.; Lions, F. *J. Am. Chem. Soc.* **1959**, *81*, 6415.
(6) Baiano, A. J.; Carlson, D. L.; Wolosh, G. M.; DeJesus, D. E.; Knowles, C. F.; Szabo, E. G.; Murphy, W. R., Jr. *Inorg. Chem.* **1990**, *29*, 2327.

0020-1669/92/1331-1594$03.00/0 